Calculated OH-Stretching Vibrational Transitions of the Water−Nitric Acid Complex

Henrik G. Kjaergaard*

Department of Chemistry, University of Otago, P.O. Box 56, Dunedin, New Zealand

Received: October 31, 2001; In Final Form: January 7, 2002

We have calculated fundamental and overtone OH-stretching vibrational band frequencies and intensities of the water−nitric acid complex. The calculations use the simple harmonically coupled anharmonic oscillator (HCAO) local-mode model with local-mode parameters obtained from scaled ab initio calculations and ab initio-calculated dipole moment functions. The ab initio calculations were performed at the HF, B3LYP, and QCISD levels of theory predominantly with the 6-311++G(2d,2p) basis set. We have compared our results for the water−nitric acid complex with results for the water dimer and the nitric acid and water molecules. The results show that the water−nitric acid complex is more strongly bound, and the changes in spectroscopic properties compared to the individual molecules are more significant than those for the water dimer. The total OH-stretching intensity of the water−nitric acid complex is significantly higher than the sum of the intensities for the individual molecules in the fundamental and higher overtone regions. The transitions associated with the hydrogen-bonded OH bond show a very large red shift compared to the OH-stretching transitions of the nitric acid molecule. These red-shifted bands provide likely spectral regions for the detection of the water−nitric acid complex in the near-infrared. The effect of the water−nitric acid complex on atmospheric OH radial productions and absorption of solar radiation is discussed.

Introduction

Vibrational spectra in the near-infrared (NIR) and visible regions are dominated by XH-stretching overtone vibrations, where X is a heavy atom like C, O, or N. The large-amplitude motion associated with XH-stretching vibrations have been explained well by the harmonically coupled anharmonic oscillator (HCAO) local-mode model.[1−5] More recently, overtone intensities have been successfully predicted with the use of vibrational wave functions obtained with the HCAO local-mode model and ab initio-calculated dipole moment functions.[6−11]

The effects of basis set size and choice of theory on vibrational band intensities have been investigated for a few smaller molecules.[12−15] We have found that relative intensities within an overtone can be predicted correctly with a modest ab initio-calculated dipole moment function at the Hartree−Fock self-consistent-field (HF) level of theory and a 6-31G(d) basis set.[10−12] We showed that an improvement of the basis set results in accurate absolute intensities and that electron correlation was predominantly necessary to get accurate intensities of the fundamental transitions. In our recent study of the water dimer, we found that both the larger basis set 6-311++G(2d,2p) and electron correlation in the form of the quadratic configuration interaction including singles and doubles (QCISD) theory seemed to improve the results in particular with regard to the hydrogen-bonded OH bond.[16] However, the computational requirements of the QCISD theory increase rapidly with increasing system size. We have recently shown for a few molecules that overtone intensities calculated with hybrid density functional theories (e.g., B3LYP) give results that are very similar to those obtained with the QCISD method provided a reasonable-sized basis set is used.[14] These B3LYP results are obtained at a substantially reduced computational cost compared to the QCISD calculations, and this makes the B3LYP calculations very attractive. However, the B3LYP method does not appear to describe the hydrogen bonds in these complexes well.

We have recently suggested a method that allows the calculation of overtone spectra of molecules for which no overtone spectra have been recorded. We have applied this method to the water dimer[16] and used the calculated spectra to assess the importance of the water dimer as an atmospheric absorber of solar radiation.[17] The calculated overtone spectrum of the water dimer clearly indicates that certain spectral regions are favorable for atmospheric and laboratory investigations of the water dimer.[16,17]

In the present paper, we have applied our recently developed method to the water−nitric acid complex. Our method of calculating overtone spectra of complexes provides a valuable guide to experiments in predicting which spectral ranges are optimal for detection of the complexes. The water−nitric acid complex seems to be well-suited for comparisons between experiment and theory and is of possible importance for the atmosphere.

Compared to the large number of studies on the water dimer, $H_2O{\cdot}H_2O$, and larger water clusters, there has been relatively little work done on the monohydrated nitric acid complex, $H_2O{\cdot}HNO_3$. Infrared (IR) spectra of $H_2O{\cdot}HNO_3$ isolated in cold matrixes have been recorded,[18,19] and the structure of the complex has been determined by microwave studies.[20] However, no vapor-phase vibrational IR or NIR spectra of $H_2O{\cdot}HNO_3$ have been observed yet. Theoretical studies have calculated the optimized geometry, harmonic vibrational frequencies, and fundamental intensities with a harmonic oscillator linear dipole approximation of the $H_2O{\cdot}HNO_3$ complex.[21−25] The calculated structures are in good agreement with the one determined by microwave spectroscopy.

* To whom correspondence should be addressed. E-mail: henrik@alkali.otago.ac.nz. Fax: 64-3-479-7906. Phone: 64-3-479-5378. On sabbatical at Cooperative Institute for Research in Environmental Sciences (CIRES), University of Colorado, Boulder, CO 80309-0216.

10.1021/jp014018n CCC: $22.00
Published on Web 03/06/2002

Recently, absolute intensities of the OH-stretching overtone transitions in the $\Delta\nu_{OH} = 3$, 4, and 5 regions of nitric acid have been recorded with conventional spectroscopy[15,26] and cavity ring down spectroscopy.[27] It was shown that the intensities of the OH-stretching transitions $\Delta\nu_{OH} = 3$, 4 in HNO_3 could be calculated well by the HCAO local-mode model and an ab initio QCISD/6-31+G(d,p) dipole moment function.[15]

In the present paper, we have calculated the OH-stretching vibrational band frequencies and intensities of the water−nitric acid complex. We have used the HCAO local-mode model with scaled ab initio-calculated local-mode parameters and ab initio-calculated dipole moment functions. The ab initio calculations were performed at the HF, B3LYP, and QCISD levels of theory with the 6-311++G(2d,2p) basis set. We have investigated our computational approach for HNO_3 and compare our results with the recently determined experimental intensities[15,26,27] and the previous calculation.[15] We compare our calculations for $H_2O{\cdot}HNO_3$ with calculations for $H_2O{\cdot}H_2O$ and the H_2O and HNO_3 molecules.

The absorption of solar radiation by the atmosphere is essential to the Earth's climate. Various water-containing clusters have been suggested to be of potential importance in the absorption of solar radiation.[28] The water dimer has been estimated to account for a nonnegligible amount of solar absorption.[17,29] The atmospheric abundance of the water−nitric acid complex has recently been estimated and was found to be less than that of the water dimer.[28] However, both abundance and the absorption spectrum of $H_2O{\cdot}HNO_3$ are required to estimate its effect on absorption of solar radiation. Certainly in polluted areas, the local concentrations of nitric acid can be significant, but on a global average it is unlikely that the water−nitric acid complex will contribute significantly to solar absorption.

The nitric acid molecule has been suggested to contribute to the atmospheric OH radical production via direct overtone photodissociation.[30] Because the atmospheric concentration of OH is very low, even small sources can be important. The efficiency of the direct overtone photodissociation process depends on the absorption intensity (cross section) of the OH-stretching overtones with sufficient energy. We show that by formation of the monohydrated complex the OH-stretching overtone transitions change significantly both in energy and in intensity. Thus, the water−nitric acid complex is likely to have a different direct overtone photodissociation level compared to the parent nitric acid molecule. We provide calculated OH-stretching spectra of $H_2O{\cdot}HNO_3$ in the regions of interest to the absorption of solar radiation and photodissociation of the complex to form OH radicals. Our calculations on the $H_2O{\cdot}HNO_3$ complex provide a guide to the spectral regions that are favorable for the detection of the water−nitric acid complex.

Theory and Calculations

The oscillator strength, *f*, of a transition from the ground vibrational state, g, to an excited state, e, is given by[10,31]

$$f_{eg} = 4.702 \times 10^{-7}\,[\mathrm{cm\ D^{-2}}]\ \tilde{\nu}_{eg}|\vec{\mu}_{eg}|^2 \qquad (1)$$

where $\tilde{\nu}_{eg}$ is the vibrational wavenumber of the transition and $\vec{\mu}_{eg} = \langle e|\vec{\mu}|g\rangle$ is the transition dipole moment matrix element in Debye (D). Thus, both vibrational wave functions and the dipole moment function are required to calculate vibrational band intensities and to simulate overtone spectra. Experimental vibrational intensities are commonly given as an absorption coefficient with units of km mol^{-1} for fundamental transitions and integrated cross sections with units of cm $molecule^{-1}$ for overtones. Conversions of the dimensionless oscillator strengths to km mol^{-1} and cm $molecule^{-1}$ are 5.33×10^6 km $mol^{-1} \times f$ and 8.85×10^{-13} cm $molecule^{-1} \times f$, respectively.

Vibrational Model. We use the HCAO local-mode model to describe OH-stretching vibrational modes in $H_2O{\cdot}HNO_3$ and $H_2O{\cdot}H_2O$ complexes and in individual H_2O and HNO_3 molecules. Overtone spectra are dominated by OH-stretching transitions, and the simple HCAO local-mode model only includes OH-stretching modes with no coupling to other vibrational modes. We have previously shown this to be a good approximation.[11,32]

Within the HCAO local-mode model, the HNO_3 molecule and the HNO_3 unit in the $H_2O{\cdot}HNO_3$ dimer are described by a single isolated OH-stretching oscillator.[11,14] The H_2O molecule and the H_2O units in the complexes are described by two harmonically coupled anharmonic OH-stretching oscillators. For the H_2O molecule and the hydrogen-acceptor H_2O unit in $H_2O{\cdot}H_2O$, the two OH bonds are equivalent and we describe them by a symmetric H_2O unit.[10,16] Asymmetric H_2O units are used to describe the hydrogen-donor H_2O unit in $H_2O{\cdot}H_2O$ and the H_2O unit in $H_2O{\cdot}HNO_3$.[16,32] The details of these models are given in previous papers, and we only give a brief outline here.[10,11,14,16,32]

The model Hamiltonian for an isolated OH-stretching Morse oscillator can be written[13]

$$(H - E_{|0\rangle})/(hc) = v\tilde{\omega} - (v^2 + v)\tilde{\omega}x \qquad (2)$$

where $E_{|0\rangle}$ is the energy of the vibrational ground state and $\tilde{\omega}$ and $\tilde{\omega}x$ are the local-mode frequency and anharmonicity (in cm^{-1}) of the OH oscillator. The eigenstates of the Hamiltonian are denoted by $|v\rangle$, where v is the vibrational quantum number and the eigenstates are Morse oscillator wave functions. The local-mode parameters, $\tilde{\omega}$ and $\tilde{\omega}x$, are usually derived from the observed local-mode peak positions. However, no overtone transitions have yet been observed for the water dimer and the water−nitric acid complex, and we have used a method based on ab initio-calculated potential energy curves to obtain the local-mode parameters [vide infra].

The model Hamiltonian for two equivalent OH-stretching oscillators is[10]

$$(H^0 - E_{|00\rangle})/(hc) = (v_1 + v_2)\tilde{\omega} - ({v_1}^2 + {v_2}^2 + v_1 + v_2)\tilde{\omega}x \qquad (3)$$

with the effective harmonic coupling limited to[10]

$$H'/(hc) = -\gamma'({a_1}^{+}a_2 + a_1{a_2}^{+}) \qquad (4)$$

where a and a^+ are the usual step-up and step-down operators known from harmonic oscillators.[33] The effective coupling parameter contains both the kinetic and potential energy coupling and is given by[10]

$$\gamma' = \left(-\frac{\cos\theta}{2}\left(\frac{m_H}{m_H + m_O}\right) - \frac{F_{12}}{2F_{11}}\right)\tilde{\omega} \qquad (5)$$

where θ is the HOH angle, m_i is the atomic masses, and F_{ij} is the force constants.[10] The model for two nonequivalent OH oscillators is similar to eqs 3−5 with the $\tilde{\omega}$ term in eq 3 split into an $\tilde{\omega}_1$ and $\tilde{\omega}_2$ term depending on the respective quantum numbers and likewise for the $\tilde{\omega}x$ terms. In eq 5, $\tilde{\omega}$ should be

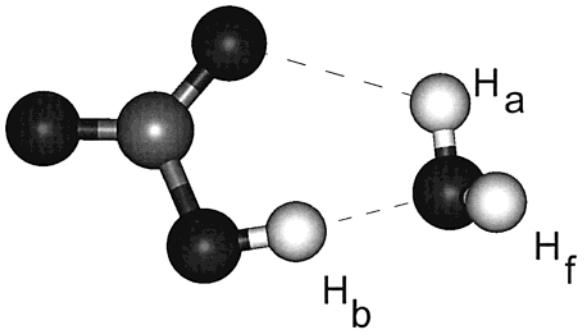

Figure 1. The QCISD/6-311++G(2d,2p) optimized structure of the $H_2O{\cdot}HNO_3$ complex and the labeling used.

replaced by $\sqrt{\tilde{\omega}_1\tilde{\omega}_2}$ and F_{11} with $\sqrt{F_{11}F_{22}}$.[32] We refer to previous papers for details.[10,16,32]

Ab Initio Determination of Local-Mode Parameters. The Morse oscillator frequency, $\tilde{\omega}$, and anharmonicity, $\tilde{\omega}x$, can be expressed in terms of the reduced mass of the oscillator and the second- and third-order ab initio-calculated force constants, F_{ii} and F_{iii}, by[16,34]

$$\tilde{\omega} = \frac{\omega}{2\pi c} = \frac{(F_{ii}G_{ii})^{1/2}}{2\pi c} \tag{6}$$

$$\tilde{\omega}x = \frac{\omega x}{2\pi c} = \frac{hG_{ii}}{72\pi^2 c}\left(\frac{F_{iii}}{F_{ii}}\right)^2 \tag{7}$$

where G_{ii} is the reciprocal of the reduced mass. The force constants are the derivatives of the potential energy, $V(q)$, with respect to the internal displacement coordinate, q. We calculate the force constants by standard numerical techniques from a one-dimensional grid of ab initio-calculated potential energies (potential energy curve), $V(q)$.[35] The grid is calculated by displacing the internal coordinate from the equilibrium position. These one-dimensional grids are also used to obtain the dipole moment function [vide infra]. Similar to the commonly used scaling of ab initio-calculated harmonic frequencies, we scale our ab initio-calculated local-mode parameters to compensate for deficiencies in the ab initio method.[16] We have used the accurate experimental local-mode parameters for H_2O to determine scaling factors that, we believe, are suitable for the water units in hydrated complexes. Average scaling factors determined from a series of acid and alcohol molecules resulted in an average scaling factor similar to the one found for H_2O. We have used the experimental local-mode parameter for HNO_3 to determine scaling factors that, we believe, are suitable for the OH_b bond of the $H_2O{\cdot}HNO_3$ complex and use the H_2O scaling factor for the OH_a and OH_f bonds in the complex. The labeling of the different hydrogen atoms in the $H_2O{\cdot}HNO_3$ complex is given in Figure 1.

Dipole Moment Function. For an isolated OH oscillator, we express the dipole moment function as a series expansion in the displacement coordinate,[11,16]

$$\vec{\mu}(q) = \sum_i \vec{\mu}_i q^i \tag{8}$$

where $\vec{\mu}_i$ is $1/i!$ times the ith-order derivative of the dipole moment function with respect to the internal displacement coordinate, q. The coefficients $\vec{\mu}_i$ are calculated by standard numerical techniques from the one-dimensional (1D) dipole moment grid, $\vec{\mu}(q)$.[35] The grid is calculated by displacing the OH bond by ± 0.2 Å from the equilibrium position in steps of 0.05 Å. This series of single-point ab initio calculations provides both $V(q)$ and $\vec{\mu}(q)$. The nine-point grid with a step size of 0.05 Å provides good convergence of the dipole moment derivatives and force constants. The choice of grid and step size is based on previous work.[16,32] We have limited the expansion of eq 8 to fifth order. The calculated intensities seem to be well-converged with the fifth-order dipole expansion for transitions up to $v = 6$. The dipole derivatives in eq 8 are essentially numerical differences, and we find that the sixth- and higher-order derivatives have significant uncertainties due to the limited numerical accuracy of the ab initio-calculated dipole moments.

For the H_2O units, we expand the dipole moment function as[10,16,32]

$$\vec{\mu}(q_1,q_2) = \sum_{i,j} \vec{\mu}_{ij}\, q_1^{\,i} q_2^{\,j} \tag{9}$$

and need to calculate a two-dimensional (2D) grid. We use the same range as for the 1D grids but limit the expansion of the 2D grids to third order in the mixed terms. Thus, 9×9 2D grids were calculated except for the QCISD/6-311++G(2d,2p) grid for the H_2O unit in $H_2O{\cdot}HNO_3$, which was limited to a 5×5 grid. The mixed derivatives mainly affect the intensities of the less-intense transitions to the local-mode combination states, and the derivatives determined from a 5×5 grid are reasonably converged. The 2D grids provide the coefficients $\vec{\mu}_{ij}$ in eq 9 as well as the mixed force constants, F_{ij}, used to determine the effective harmonic coupling parameter (eq 5).

The optimized geometries and all points in a grid were calculated at a specified ab initio method with the use of Gaussian 94.[36] Values of the dipole moment are calculated with use of the generalized density for the specified level of theory, which will provide dipole moments that are the correct analytical derivatives of the energy. All B3LYP calculations were run with an increased integration grid size (Keyword Int=99434) to improve the convergence of the higher-order dipole derivatives.[37]

Results and Discussion

The QCISD/6-311++(2d,2p) optimized geometry of the $H_2O{\cdot}HNO_3$ complex is shown in Figure 1. Our B3LYP/6-311++G(2d,2p) optimized geometry is close to the MP2 calculated geometries of Tso et al.[22] and Toth,[24] which are all in agreement with the microwave-determined structure.[20] The QCISD/6-311++(2d,2p) optimized geometry is similar to that determined at both the B3LYP and MP2 levels[22−25] but agrees slightly better with the experimental microwave data.[20] The $H_b{\cdot}{\cdot}{\cdot}O$ distance between the two units is measured to be 1.779 Å and calculated with the QCISD/6-311++G(2d,2p) method to be 1.748 Å compared to about 1.70−1.71 Å for the various B3LYP and MP2 calculations.[22−25] The QCISD calculation also predicts a significantly shorter OH_b bond compared to the B3LYP and MP2 calculations. The QCISD calculated $H_a{\cdots}O$ distance is 2.43 Å, which is close to the distance of 2.49 Å estimated from the microwave experiment.[20] In the Supporting Information Figures 1S and 2S and Tables 1S−4S, we give the full set of optimized parameters for the structures studied.

In Table 1, we have given the QCISD/6-311++(2d,2p)-calculated OH bond lengths of the monomer units H_2O and HNO_3 and the complexes $H_2O{\cdot}H_2O$ and $H_2O{\cdot}HNO_3$. Compared to the monomer units, the OH_b bond is lengthened by 16 mÅ and the OH_a bond by 4 mÅ in the $H_2O{\cdot}HNO_3$ complex. By comparison, the hydrogen-bonded OH_b bond in $H_2O{\cdot}H_2O$ is lengthened by 5 mÅ,[16] and the OH_b-stretching fundamental

TABLE 1: Calculated OH Bond Lengths (Å)[a]

bond	$H_2O{\cdot}HNO_3$	H_2O	HNO_3	$H_2O{\cdot}H_2O$[b]
OH_f	0.957	0.956		0.956
OH_a	0.960	0.956		0.957
OH_b	0.982		0.966	0.961

[a] Calculated with the QCISD/6-311++G(2d,2p) method. [b] The OH bond labels are OH_a for the two equivalent OH bonds on the hydrogen acceptor H_2O unit and OH_b and OH_f for the two nonequivalent OH bonds on the hydrogen donator H_2O unit.

transition is observed to be significantly red-shifted compared to the other OH-stretching transitions.[38] We would expect to observe a significant red shift of the OH_b- and OH_a-stretching transitions in the $H_2O{\cdot}HNO_3$ complex. Overtone transitions of bonds with calculated bond lengths that differ by as little as 1 mÅ are typically well-resolved.[10] That the three OH bonds in $H_2O{\cdot}HNO_3$ have different OH bond lengths suggests that overtone transitions to all three could be observed. The lengthening of the OH_a bond suggests a partial hydrogen bond between H_a and the adjacent O in the HNO_3 unit, as previously suggested.[22]

The QCISD/6-311++G(2d,2p)-calculated H_aOH_f angle in $H_2O{\cdot}HNO_3$ is 105.4° compared to 104.5° in the H_2O molecule and 104.8° and 104.9° in the acceptor and donor units of $H_2O{\cdot}H_2O$, respectively. Thus, the kinetic coupling between the OH-stretching oscillators will be similar in these four H_2O units and the HOH-bending vibrational frequencies are expected to be similar.

The B3LYP/6-311++G(2d,2p) and QCISD/6-311++G(2d,2p)-calculated binding energies of the $H_2O{\cdot}HNO_3$ complex are 40.4 and 41.8 kJ/mol, respectively, similar to the previous MP2 and B3LYP results.[22-25] The counterpoise basis set superposition error (BSSE) correction[39] lowers the B3LYP/6-311++G(2d,2p) binding energy by about 1 kJ/mol. The B3LYP/6-311++G(2d,2p) BSSE-corrected binding energy of $H_2O{\cdot}H_2O$ is 19.3 kJ/mol in agreement with the experimental value of about 22.6 ± 2.9 kJ/mol.[40] The larger binding energy of $H_2O{\cdot}HNO_3$ compared to $H_2O{\cdot}H_2O$ indicates a stronger hydrogen bond and is observed in the significantly shorter $H_b{\cdot}{\cdot}{\cdot}O$ distance (1.75 Å vs 1.98 Å) and longer OH_b bond (0.982 Å vs 0.961 Å) in the $H_2O{\cdot}HNO_3$ complex.

Fundamental Vibrations. The B3LYP/6-311++G(2d,2p)-calculated fundamental harmonic frequencies and band intensities of selected vibrational modes in H_2O, HNO_3, $H_2O{\cdot}H_2O$, and $H_2O{\cdot}HNO_3$ are given in Table 2. Our calculated results are in agreement with previous results.[22-25] Calculated harmonic frequencies are not expected to agree well with the observed IR transition frequencies, in particular, for modes with significant anharmonicity. The OH-stretching fundamental transition in HNO_3 is observed at 3551.6 cm^{-1},[41] which is close to the calculated harmonic frequency of 3733 cm^{-1}, if a reasonable OH-stretching anharmonicity of about 90 cm^{-1} is assumed. Similarly if the anharmonicity of the NOH-bending mode in HNO_3 is estimated to be about 20 cm^{-1}, its calculated frequency agrees quite well with the observed IR transition frequency of 1303 cm^{-1}.[42]

The water dimer has four IR active OH-stretching vibrations. The calculated harmonic frequency of the OH_f- and OH_a-stretching transitions agrees well with recent experiments, if the anharmonicity is considered.[38,43] The OH-stretching transitions involved in hydrogen bonding are commonly red-shifted.[44] If anharmonicity is considered, the B3LYP-calculated OH_b-stretching harmonic frequency in Table 2 is significantly lower than the observed transition at 3601 cm^{-1}.[38] This suggests that the B3LYP theory overestimates the frequency red shift of OH-stretching vibrations involved in hydrogen bonding in agreement with other calculations.[44] The HOH-bending vibrations seem to be only slightly affected by the formation of the $H_2O{\cdot}H_2O$ complex, as expected by the very similar HOH angles.

Formation of the $H_2O{\cdot}HNO_3$ complex affects predominantly the OH_b-stretching and NOH_b-bending mode compared to the isolated molecules. It is not surprising that the two vibrational normal modes most affected by the formation of the complex are the two modes that involve the hydrogen atom H_b, which participates in hydrogen bonding. The calculated harmonic frequency of the NOH_b-bending mode increases by about 100 cm^{-1}, and that of the OH_b-stretching mode decreases by about 500 cm^{-1} on formation of the complex. The calculated increase in the frequency of the NOH_b-bending mode is in good agreement with experimental matrix isolations IR studies.[18,19] The calculated red shift of the OH_b-stretching vibration resembles the shift observed in argon matrix spectra; however, the observed OH-stretching region is complicated by the occurrence of several bands.[19] The difference in harmonic frequency between the OH_b-stretching vibration in HNO_3 and $HNO_3{\cdot}H_2O$ is large compared to the corresponding difference in anharmonicity, and thus, the anharmonicity will have little effect on the observed and calculated shifts. It is somewhat surprising that the B3LYP results agree well with the observed frequency shifts considering the lack of agreement for the OH_b-stretching vibration in the water dimer for which the transition frequency is accurately determined.[38] The OH-stretching transition in HNO_3 is red-shifted by about 30 and 60 cm^{-1} in the Ar and N_2 matrix spectra, respectively, compared to the vapor-phase spectrum.[18,19,41,45] It is possible that the matrix perturbs the complexes and red shifts the OH_b transition in $HNO_3{\cdot}H_2O$ more than the OH-stretching transition in HNO_3. Unfortunately, no vapor-phase spectra of the $H_2O{\cdot}HNO_3$ complex are available, and furthermore, the additional spectral structure in the argon matrix spectra makes the assignment of the OH-stretching vibrations difficult.[19]

We have calculated the harmonic frequencies for the nitric acid dimer $(HNO_3)_2$ with the B3LYP/6-311++G(2d,2p) method. The nitric acid dimer has a smaller binding energy than the $H_2O{\cdot}HNO_3$ complex and also a slightly shorter OH_b bond length. The OH_b-stretching transition is observed to be less red-shifted than the transition in the $H_2O{\cdot}HNO_3$ complex in the N_2 and argon matrix isolation spectra, as expected.[19,45] The B3LYP calculated shifts are comparable to the observed shift in the matrix spectra. We suggest again that the matrix is perturbing the nitric acid dimer more than the monomer rather than that the B3LYP method is providing good OH_b-stretching frequencies.

The most significant change in calculated intensities on complex formation is the large increase in intensity of the OH_b-stretching transition. In $H_2O{\cdot}HNO_3$, the intensity of the OH_b-stretching transitions is about 10 times stronger than that in HNO_3. The intensity of the OH_b-stretching transition is about three times stronger in $H_2O{\cdot}HNO_3$ than in $H_2O{\cdot}H_2O$, in agreement with the stronger hydrogen bond in the $H_2O{\cdot}HNO_3$ complex. The OH_a- and OH_f-stretching vibrations in $H_2O{\cdot}HNO_3$ are about twice as intense as the symmetric and asymmetric OH-stretching transitions in H_2O. The NO-stretching vibrations show little change in intensity on complex formation apart from intensity shifts between the NO_2 symmetric- and asymmetric-stretching vibrations. This is anticipated because the symmetry of the molecule changes when the complex is formed.

Scaling Factors and Local-Mode Parameters. In our previous paper on $H_2O{\cdot}H_2O$, we compared results obtained with

TABLE 2: Calculated Harmonic Frequencies (cm^{-1}) and Band Intensities (km mol^{-1}) of Selected Fundamental Vibrations in $H_2O{\cdot}HNO_3$, H_2O, HNO_3, and $H_2O{\cdot}H_2O$[a]

	$\tilde{\nu}$				intensity			
mode	$H_2O{\cdot}HNO_3$	HNO_3	H_2O	$H_2O{\cdot}H_2O$	$H_2O{\cdot}HNO_3$	HNO_3	H_2O	$H_2O{\cdot}H_2O$
NO str	945	903			150	185		
NO_2 s-str[b]	1326	1323			256	75		
NOH bend[b]	1476	1347			247	304		
HOH bend	1632		1640	1641/1660[c]	165		71	96/33[c]
NO_2 a-str	1736	1738			261	414		
OH_b str	3243	3733		3704	1101	100		330
OH_a str	3787		3821	3813/3912[d]	31		8	14/84[d]
OH_f str	3895		3923	3894	116		62	85

[a] Calculated with the B3LYP/6-311++G(2d,2p) method within Gaussian 94. Frequencies reported are unscaled harmonic frequencies. [b] These two modes are strongly mixed. [c] The HOH-bending mode of the donor and acceptor H_2O units, respectively. [d] The symmetric and asymmetric OH-stretching vibrations in the H_2O acceptor unit, respectively.

TABLE 3: Calculated Local-Mode Frequencies (cm^{-1})[a]

bond	$H_2O{\cdot}HNO_3$	H_2O	HNO_3	$H_2O{\cdot}H_2O$
OH_f	3868	3870		3878
OH_a	3833	3870		3862
OH_b	3380		3708	3781

[a] Calculated with the QCISD/6-311++G(2d,2p) method. The calculated frequencies have been scaled by 0.9836 for the OH bonds in the H_2O units and by 0.9743 for OH bonds in the HNO_3 units. This scaling yields the experimental value of 3870 cm^{-1} for H_2O and 3708 cm^{-1} for HNO_3.

TABLE 4: Calculated Local-Mode Anharmonicities (cm^{-1})[a]

bond	$H_2O{\cdot}HNO_3$	H_2O	HNO_3	$H_2O{\cdot}H_2O$
OH_f	81.4	82.1		82.2
OH_a	81.1	82.1		81.7
OH_b	99.8		78.9	85.4

[a] Calculated with the QCISD/6-311++G(2d,2p) method. The calculated anharmonicities have been scaled by 0.850 for the OH bonds in the H_2O units and by 0.819 for the OH bonds in the HNO_3 units. This scaling yields the experimental value of 82.1 cm^{-1} for H_2O and 78.9 cm^{-1} for HNO_3.

HF and QCISD methods.[16] In general, similar $\tilde{\omega}$ and $\tilde{\omega}x$ values were predicted for the three nonequivalent OH bonds in the water dimer with the two theories and the 6-31G(d), 6-311+G(d,p), and 6-311++G(2d,2p) basis sets. The variation in the calculated parameters was slightly larger with the 6-31G(d) basis set. In the present paper, we have calculated $\tilde{\omega}$ and $\tilde{\omega}x$ values using the HF, B3LYP, and QCISD theories and the 6-311++G(2d,2p) basis set. The local-mode parameters calculated with the QCISD/6-311++G(2d,2p) method for the $H_2O{\cdot}HNO_3$ and $H_2O{\cdot}H_2O$ complexes are given in Tables 3 and 4. We have scaled the ab initio-calculated parameters with scaling factors found from the water and nitric acid experimental data. The scaling factors used are given in the footnotes to the tables. The local-mode parameters calculated with the other methods are given as Supporting Information in Tables 5S−10S.

We have determined the experimental frequency and anharmonicity of the OH-stretching oscillator in HNO_3 to be 3708 and 78.9 cm^{-1}, respectively, from the published fundamental and $\Delta\nu_{OH} = 3-6$ overtone transition frequencies.[15,41,46−48] Some of the experimentally determined transition frequencies are not given accurately in the papers, and we estimate the uncertainty in the determined local-mode frequency and anharmonicity to be about 5 and 2 cm^{-1}, respectively. The observed and calculated OH-stretching transition frequencies are given in Table 5. The agreement between observed and calculated frequencies is good, however, with larger disagreement for the higher overtones perhaps suggesting deviation from a Morse potential. The experimentally derived OH-stretching local-mode

TABLE 5: Observed and Calculated OH-Stretching Frequencies (cm^{-1}) in HNO_3

υ	observed	calculated[a]
1	3551.6[b]	3549.8
2		6941.8
3	10 173[c]	10 175.8
4	13 245[c], 13 248[d], 13 250[e]	13 252.0
5	16 160[f]	16 170.3
6	18 950[f]	18 930.7

[a] Calculated with the experimental local-mode parameters given in Tables 3 and 4. [b] Reference 41. [c] Reference 15. [d] Reference 46, value used in Birge−Spooner fit. [e] Reference 48. [f] Reference 47. For $\upsilon = 5$, 16 160 cm^{-1} is the value given in the text and used in our fit. The value 16 166 cm^{-1} is given in a figure caption of ref 47.

frequency and anharmonicity for H_2O are 3870 and 82.1 cm^{-1}, respectively.[49]

The ab initio-calculated and H_2O-scaled frequency for HNO_3 is 3732 and 3743 cm^{-1} with the B3LYP and QCISD theories, respectively, and 3770 cm^{-1} with the HF theory. The calculated and scaled values of the local-mode anharmonicity for the OH-stretching oscillator in HNO_3 are similar with the three methods and compare well with the experimental value.

We tested the sensitivity of the B3LYP-calculated OH-stretching local-mode parameters in HNO_3 with basis-set size. We included the 6-311++G(2d,2p), 6-311++G(3d,3p), 6-311++G(3df,3pd), aug-cc-pVDZ, and aug-cc-pVTZ basis sets. The calculated $\tilde{\omega}$ and $\tilde{\omega}x$ values were scaled with scaling factors appropriate to the given ab initio method and found from comparison with H_2O results. Interestingly, the calculated values of $\tilde{\omega}$ and $\tilde{\omega}x$ with this range of basis sets are all within $\tilde{\omega} = 3732 \pm 1$ cm^{-1} and $\tilde{\omega}x = 82.7 \pm 0.3$ cm^{-1}. This variation is significantly less than what we have found previously with basis sets smaller than 6-311++G(2d,2p).[16] Thus, on the basis of the calculated local-mode parameters, there seems to be little advantage in increasing the basis set beyond the 6-311++G(2d,2p) basis set.

The calculated $\tilde{\omega}$ and $\tilde{\omega}x$ values for the OH_a and OH_f bonds in the water dimer are very similar with HF, B3LYP, and QCISD theories and the 6-311++G(2d,2p) basis set. For the hydrogen-bonded OH_b bond, HF and QCISD methods give similar local-mode parameters, which lead to predicted fundamental frequencies[16] that are in good agreement with the experimentally observed values.[38,43] However, the $\tilde{\omega}$ value obtained with the B3LYP method is about 70 cm^{-1} smaller and the $\tilde{\omega}x$ value about 5 cm^{-1} larger than those obtained with the HF and QCISD methods. The B3LYP results lead to fundamental frequencies that are not in agreement with the experiments.[38,43] It has been observed that various DFT theories including B3LYP overestimate the red shift of the hydrogen-

TABLE 6: Calculated and Observed Oscillator Strengths of the OH-Stretching Transitions in HNO_3

	calculated					
v	HF[b]	B3LYP[b]	QCISD[b]	QCISD[c]	observed[a]	exponent
1	3.08	1.69	1.73			−5
2	4.57	6.01	6.05	6.85		−7
3	1.98	2.95	2.26	2.78	2.9, 3.2	−8
4	1.36	1.80	1.41	2.14	2.7, 2.5, 3.2	−9
5	1.35	1.51	1.36	2.55	2.9	−10
6	1.72	1.73	1.75	3.46		−11

[a] Observed values from refs 15, 26, and 27 and converted to oscillator strengths. [b] With the 6-311++G(2d,2p) basis set and the experimental local-mode parameters. [c] From ref 15. QCISD/6-31+G(d,p) calculated dipole moment function and experimental local-mode parameters.

TABLE 7: Basis Set Variation of B3LYP-Calculated Oscillator Strengths of the OH-Stretching Transitions in HNO_3

	calculated[a]						
v	III[c]	IV[d]	V[e]	VDZ[f]	VTZ[g]	observed[b]	exponent
1	1.69	1.60	1.61	1.59	1.59		−5
2	6.01	5.51	5.41	5.39	5.48		−7
3	2.95	2.72	2.58	2.68	2.68	2.9, 3.2	−8
4	1.80	1.75	1.93	1.56	1.57	2.7, 2.5, 3.2	−9
5	1.51	1.66	2.18	1.12	1.34	2.9	−10
6	1.73	2.18	3.31	1.19	1.68		−11

[a] Calculated with the experimental local-mode parameters. [b] Observed values from refs 15, 26, and 27 and converted to oscillator strengths. [c] Basis set 6-311++G(2d,2p). [d] Basis set 6-311++G(3d,3p). [e] Basis set 6-311++G(3df,3pd). [f] Basis set aug-cc-pVDZ. [g] Basis set aug-cc-pVTZ.

bonded stretching vibration.[44] Recently, new functionals like HCTH have been proposed that seem to somewhat improve the results for water dimer.[50] Despite the slight improvement, the frequency of the OH_b-stretching transitions are still predicted too low.[50,51] Thus, it seems that the computationally favorable B3LYP method is not a suitable choice for the calculation of OH_b-stretching vibrations in hydrogen-bonded systems. We also indicated that the HF method does not seem like the best choice of method for calculations involving nitric acid. Thus, we suggest that it is necessary to use the resource-demanding QCISD method. The QCISD/6-311++G(2d,2p) calculations for $H_2O{\cdot}HNO_3$ required about 9.6 Gb of scratch disk space.

On the basis of the calculations for water dimer and nitric acid, we estimate the error in $\tilde{\omega}$ and $\tilde{\omega}x$ to be less than 30 and 3 cm^{-1}, respectively. The use of separate scaling factors for OH_b and the other OH bonds probably leads to even less uncertainty. The uncertainty in $\tilde{\omega}$ leads to a significant uncertainty in peak positions; however, the uncertainty in $\tilde{\omega}x$ leads to only a modest uncertainty in the intensities.

Intensities of OH-Stretching Transitions in HNO_3. We have calculated the OH-stretching intensities in HNO_3 to investigate the accuracy of our simple model on a system relevant to the $H_2O{\cdot}HNO_3$ complex. The absolute intensities of the OH-stretching transition in HNO_3 have recently been measured in the $\Delta v_{OH} = 3-5$ regions.[15,26,27] The various experimental intensities agree quite well with each other as can be seen in Tables 6 and 7. The experimental uncertainties were reported by Donaldson et al.[15] and Brown et al.[27] to be about 10% and by Zhang et al.[26] to be about 30%.

The intensities calculated with the HF, B3LYP, and QCISD theories and the 6-311++G(2d,2p) basis set together with the intensities calculated by Donaldson et al.[15] are given in Table 6. The inclusion of electron correlation in the form of either the B3LYP or the QCISD theory is most important for the fundamental and lower overtones region, in agreement with previous observations.[12−14] Comparison with intensities calculated with smaller basis sets and with the previous QCISD/6-31+G(d,p) calculation shows the usual trend that a larger basis set lowers the calculated overtone intensities.[12,14] For H_2O, the intensities calculated with the QCISD/6-31+G(d,p) method are significantly higher than experimental intensities, whereas the QCISD/6-311++G(2d,2p) method yields intensities that are in good agreement with the experimental intensities.[12] Our QCISD-calculated intensities are 25−50% lower than the reported experimental intensities for the $\Delta v_{OH} = 3-5$ regions. The previous QCISD/6-31+G(d,p) calculation seems closer to the experimental values.[15] We suspect that the somewhat better agreement of the previous QCISD/6-31+G(d,p) calculation is due to cancellations arising from an imperfect dipole moment function and potential energy curve.

Calculated OH-stretching intensities of HNO_3 with a few larger basis sets and the B3LYP level of theory are shown in Table 7. The variation in intensity with basis set increases with increasing overtone. Almost identical results are obtained for the fundamental region, but the variation is almost a factor of 3 for the $\Delta v_{OH} = 6$ transition. The agreement with the experimentally determined absolute intensities for $\Delta v_{OH} = 3$ transition is quite good with all basis sets. The addition of more polarization functions to the 6-311++G(2d,2p) basis set to get the 6-311++G(3d,3p) and 6-311++G(3df,3pd) basis sets leads to improved agreement of the intensities of the $\Delta v_{OH} = 4$ and 5 transitions. The aug-cc-pVDZ and aug-cc-pVTZ basis sets give surprisingly similar results. It is interesting that even with the quite large basis sets 6-311++G(3df,3pd) and aug-cc-pVTZ the calculated intensities for the $\Delta v_{OH} = 4$ and 5 transitions are still significantly lower than the observed values. Perhaps this suggest that an improved potential beyond the Morse potential is required to obtain very accurate intensities for the higher overtones.[52]

We estimate that the use of a QCISD/6-311++G(2d,2p)-calculated DMF and ab initio-scaled local-mode parameters will lead to intensities and frequencies of OH-stretching transition with $\Delta v_{OH} \leq 6$ that will have less than a factor of 2 uncertainty in the intensities and less than 1% uncertainty in peak positions. These results can provide a useful reference to experimental efforts in observing complexes and provide suitable parameters necessary to estimate the atmospheric effect of such complexes.

Overtone Transitions in $H_2O{\cdot}H_2O$. We have calculated the frequency and intensity of the OH-stretching transitions in $H_2O{\cdot}H_2O$. Results obtained with the HF/6-311++G(2d,2p) and QCISD/6-311++G(2d,2p) methods agree with our previously published results.[16] The QCISD/6-311++G(2d,2p) results for the OH_b-stretching transitions and for the OH-stretching transitions of the symmetric hydrogen-acceptor unit are given in Tables 8 and 9, respectively, to facilitate comparison with our present results on $H_2O{\cdot}HNO_3$.

Figure 2 shows simulated overtone spectra of the water dimer in the $\Delta v_{OH} = 4$ region. The spectra were calculated with the HF, B3LYP, and QCISD theories and the 6-311++G(2d,2p) basis set. The figure clearly shows the effect of the aforementioned significantly lower $\tilde{\omega}$ value predicted for the OH_b oscillator with the B3LYP method. The band arising from the OH_b bond is red-shifted significantly more in the B3LYP simulated spectrum compared to the other two simulated spectra. The exaggerated red shifts obtained with the B3LYP theory suggest that the B3LYP theory is less suitable for hydrogen-bonded complexes. Comparison of intensities in the simulated

TABLE 8: Calculated OH_b-Stretching Transitions in $H_2O{\cdot}HNO_3$[a]

	$H_2O{\bullet}HNO_3$		$H_2O{\bullet}H_2O$[b]		HNO_3	
v	$\tilde{\nu}$, cm^{-1}	f	$\tilde{\nu}$, cm^{-1}	f	$\tilde{\nu}$, cm^{-1}	f
1	3180	1.98×10^{-4}	3594	4.88×10^{-5}	3550	1.73×10^{-5}
2	6161	1.02×10^{-7}	7035	2.03×10^{-10}	6942	6.05×10^{-7}
3	8942	1.45×10^{-8}	10 305	1.84×10^{-9}	10 176	2.26×10^{-8}
4	11 524	1.79×10^{-9}	13 404	3.44×10^{-10}	13 252	1.41×10^{-9}
5	13 906	3.78×10^{-10}	16 331	4.98×10^{-11}	16 170	1.36×10^{-10}
6	16 088	7.86×10^{-11}	19 088	7.48×10^{-12}	18 931	1.75×10^{-11}

[a] Calculated with the local-mode parameters from Tables 3 and 4 and QCISD/6-311++G(2d,2p) dipole moment functions. [b] Transitions to the $|v\rangle_b|0\rangle_f$ states of the hydrogen donor H_2O unit in $H_2O{\cdot}H_2O$ calculated with an effective coupling parameter $\gamma'_{bf} = 43.8$ cm^{-1}.

TABLE 9: Calculated OH-Stretching Transitions of the Water Unit in $H_2O{\cdot}HNO_3$[a]

	$H_2O{\cdot}HNO_3$		$H_2O{\cdot}H_2O$[b]		H_2O[b]	
state[b]	$\tilde{\nu}$, cm^{-1}	f	$\tilde{\nu}$, cm^{-1}	f	$\tilde{\nu}$, cm^{-1}	f
$\|1\rangle_a\|0\rangle_f$	3645	4.24×10^{-6}	3653	2.59×10^{-6}	3656	1.11×10^{-6}
$\|0\rangle_a\|1\rangle_f$	3731	1.60×10^{-5}	3745	1.18×10^{-5}	3755	7.88×10^{-6}
$\|2\rangle_a\|0\rangle_f$	7162	1.72×10^{-7}	7193	1.50×10^{-7}	7200	1.24×10^{-7}
$\|0\rangle_a\|2\rangle_f$	7231	5.42×10^{-7}	7235	6.09×10^{-7}	7247	6.28×10^{-7}
$\|1\rangle_a\|1\rangle_f$	7409	2.14×10^{-9}	7440	1.57×10^{-9}	7457	1.25×10^{-9}
$\|3\rangle_a\|0\rangle_f$	10 514	4.80×10^{-9}	10 582	1.02×10^{-9}	10 596	1.10×10^{-9}
$\|0\rangle_a\|3\rangle_f$	10 609	1.06×10^{-8}	10 592	1.68×10^{-8}	10 608	1.99×10^{-8}
$\|4\rangle_a\|0\rangle_f$	13 700	2.46×10^{-10}	13 798	3.61×10^{-11}	13 816	2.11×10^{-11}
$\|0\rangle_a\|4\rangle_f$	13 827	3.52×10^{-10}	13 799	6.81×10^{-10}	13 818	8.34×10^{-10}
$\|5\rangle_a\|0\rangle_f$	16 723	2.86×10^{-11}	16 845	1.93×10^{-11}	16 868	1.35×10^{-11}
$\|0\rangle_a\|5\rangle_f$	16 882	2.87×10^{-11}	16 845	4.84×10^{-11}	16 868	6.03×10^{-11}
$\|6\rangle_a\|0\rangle_f$	19 583	4.40×10^{-12}	19 728	3.37×10^{-12}	19 753	2.08×10^{-12}
$\|0\rangle_a\|6\rangle_f$	19 773	4.06×10^{-12}	19 728	5.97×10^{-12}	19 753	7.60×10^{-12}

[a] Calculated with the local-mode parameters from Tables 3 and 4, QCISD/6-311++G(2d,2p) dipole moment functions, and effective coupling parameters $\gamma'_{af} = 39.9$ cm^{-1}, $\gamma'_{aa} = 46.1$ cm^{-1}, and $\gamma' = 49.4$ cm^{-1} for $H_2O{\cdot}HNO_3$, $H_2O{\cdot}H_2O$, and H_2O, respectively. [b] The states in H_2O and the hydrogen-acceptor H_2O unit in $H_2O{\cdot}H_2O$ should be labeled $|v0\rangle_+$ and $|v0\rangle_-$ with the symmetric transitions at lower energy.

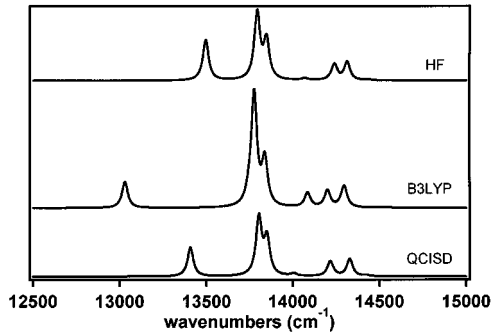

Figure 2. Simulated spectra of the $\Delta\nu_{OH} = 4$ region in water dimer. The spectra were calculated with the local-mode parameters obtained from HF, B3LYP, and QCISD calculations with the 6-311++G(2d,2p) basis set. Each vibrational transition was convoluted with a Lorentzian with a fwhm of 40 cm^{-1}.

spectra also shows the HF and QCISD results to be similar and somewhat different from the B3LYP results.

The effective coupling parameters for the H_2O units of $H_2O{\cdot}H_2O$ and $H_2O{\cdot}HNO_3$ have been calculated ab initio according to eq 5 and are given in the footnotes to Tables 8 and 9 for the QCISD/6-311++G(2d,2p) method and as Supporting Information in Tables 11S and 12S for the other methods used.

OH-Stretching Transitions in $H_2O{\cdot}HNO_3$. In Table 8, we compare the frequencies and intensities of the OH_b-stretching transitions in $H_2O{\cdot}HNO_3$ with those of OH-stretching transitions in the HNO_3 molecule and of OH_b-stretching transitions of the hydrogen-donor H_2O unit in the water dimer. As seen in Table 8, the OH_b-stretching transitions in $H_2O{\cdot}HNO_3$ are significantly red-shifted compared to those in HNO_3, as expected. The red shift in $H_2O{\cdot}HNO_3$ is significantly larger than the red shifts that we calculated for the water dimer.[16] In the $\Delta\nu_{OH} = 4$ region, the shift in $H_2O{\cdot}HNO_3$ is about 1700 cm^{-1}. Such a large shift will move the OH_b-stretching band arising from the complex into regions with possibly little absorption from the parent molecules and would facilitate detection of the complex. The OH-stretching intensities in the HNO_3 molecule are stronger than those in the H_2O molecule on a per OH bond basis. The intensity of the OH_b-stretching transition in both $H_2O{\cdot}HNO_3$ and $H_2O{\cdot}H_2O$ is significantly increased for the fundamental and higher overtones ($\Delta\nu_{OH} = 4-6$) compared to those of the HNO_3 and H_2O molecules, respectively. For the water dimer, we noticed a significant drop in the intensity of the OH_b-stretching transition in the $\Delta\nu_{OH} = 2$ region, compared to the water molecule.[16] As seen in Table 8, we predict the intensity of the OH_b-stretching transition in water dimer at $\Delta\nu_{OH} = 2$ to be weaker than the intensities of the $\Delta\nu_{OH} = 3$ and 4 transitions. Similarly, the OH_b-stretching transitions in the $\Delta\nu_{OH} = 2$ and 3 region of the $H_2O{\cdot}HNO_3$ complex are weaker than those in HNO_3. However, for the $\Delta\nu_{OH} = 2$ region, the drop in intensity in $H_2O{\cdot}HNO_3$ is not nearly as extreme as what we have seen for the water dimer. The significant drop in intensity of the OH_b-stretching transition in the $\Delta\nu_{OH} = 2$ region arises from a cancellation of almost equal contributions from the first- and second-order terms in the dipole moment expansion.

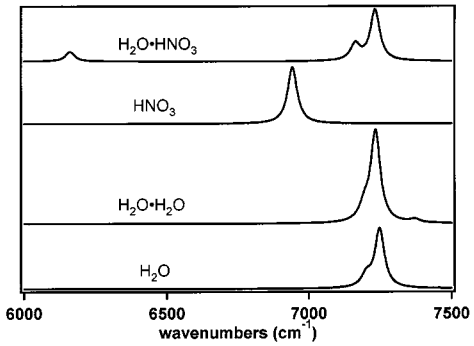

Figure 3. The simulated spectra of $H_2O{\cdot}HNO_3$, HNO_3, $H_2O{\cdot}H_2O$, and H_2O in the $\Delta\nu_{OH} = 2$ region. The spectra were calculated with the local-mode parameters from Tables 3 and 4 and QCISD/6-311++G(2d,2p) dipole moment functions. Each vibrational transition was convoluted with a Lorentzian with a fwhm of 40 cm^{-1}.

The calculated OH-stretching transitions provide a helpful guide to the experiments. Observation of the OH_b-stretching transition in the $\Delta\nu_{OH} = 2$ region of the water dimer is not likely. Recent NIR spectra in the $\Delta\nu_{OH} = 2$ region of H_2O trapped in Ar and N_2 matrixes provided OH-stretching spectra of water dimer but failed to observe the OH_b-stretching transition in agreement with our theoretical predictions.[16,53,54] However, the $\Delta\nu_{OH} = 2$ region seems suitable to observe the OH_b-stretching transition in the $H_2O{\cdot}HNO_3$ complex, a result that is not intuitively obvious. Simulated spectra of the OH-stretching transitions in the $\Delta\nu_{OH} = 2$ region for H_2O, $H_2O{\cdot}H_2O$, HNO_3, and $H_2O{\cdot}HNO_3$ are shown in Figure 3. Each vibrational transition has been convoluted with a 40 cm^{-1} wide Lorentzian band shape for ease of comparison. The H_2O spectrum has rotational structure that will spread the intensity to many sharp transitions. The $H_2O{\cdot}H_2O$ and $H_2O{\cdot}HNO_3$ transitions will more likely be Lorentzian band shapes with a full width at half-maximum (fwhm) of about 40 cm^{-1}, similar to the observed width of the $\Delta\nu_{OH} = 4$ and 5 transitions in HNO_3.[15,26,27]

TABLE 10: Calculated Total OH-Stretching Oscillator Strengths[a]

v	$H_2O{\cdot}HNO_3$	$H_2O{\cdot}H_2O$	HNO_3	H_2O	exponent
1	21.8	8.00	1.73	0.90	−5
2	8.18	11.8	6.05	7.54	−7
3	3.28	3.70	2.26	2.53	−8
4	2.58	2.03	1.41	1.15	−9
5	4.50	1.88	1.36	0.98	−10
6	8.88	2.55	1.75	1.22	−11

[a] Calculated with the local-mode parameters from Tables 3 and 4 and QCISD/6-311++G(2d,2p) dipole moment functions. The calculated effective coupling parameters are $\gamma'_{af} = 39.9$ cm^{-1} for $H_2O{\cdot}HNO_3$, $\gamma'_{aa} = 46.1$ cm^{-1} and $\gamma'_{bf} = 43.8$ cm^{-1} for $H_2O{\cdot}H_2O$ and $\gamma' = 49.4$ cm^{-1} for H_2O.

In Table 9, we compare the frequencies and intensities of the OH-stretching transitions in the H_2O unit of the $H_2O{\cdot}HNO_3$ complex with those of OH-stretching transitions in the hydrogen-acceptor H_2O unit in the water dimer and the H_2O molecule. The notation for vibrational states is suitable for the asymmetric H_2O unit in $H_2O{\cdot}HNO_3$. The H_2O molecule and the hydrogen-acceptor H_2O unit (H_aOH_a) in the water dimer are symmetric H_2O units, and the vibrational states should be labeled according to the symmetry as $|v0\rangle_+$ or $|v0\rangle_-$. The frequency of the OH_a and OH_f stretching oscillators in $H_2O{\cdot}HNO_3$ are significantly different with the OH_a frequency lower. The intensity of the OH_a-stretching fundamental transition is not enhanced as much as the OH_f transition; however, both are larger than the transitions in both H_2O and the H_aOH_a unit in water dimer. Transitions to the $|v0\rangle_+$ and $|v0\rangle_-$ states in H_2O and the H_aOH_a unit in the water dimer merge as v increases, whereas the OH_a- and OH_f-stretching transitions in $H_2O{\cdot}HNO_3$ move further apart. In the fundamental region, the state labeled $|1\rangle_a|0\rangle_f$ has a significant component of the $|0\rangle_a|1\rangle_f$ state; however, this mixing quickly disappears as v increases. In the $\Delta\nu_{OH} = 6$ region, the $|6\rangle_a|0\rangle_f$ state is 99% pure. The OH-stretching intensities are larger in $H_2O{\cdot}HNO_3$ and $H_2O{\cdot}H_2O$ than in H_2O. As v increases, the intensities of the various H_2O units become similar to that of the H_2O molecule. The intensity distribution between the two pure local-mode states is more evenly spread in the H_2O unit in $H_2O{\cdot}HNO_3$ than in the H_2O molecule or the H_aOH_a unit in water dimer.

Table 10 gives the calculated total OH-stretching oscillator strength of the molecules and complexes investigated. The total OH-stretching intensity is stronger in HNO_3 than in H_2O on a per OH bond basis. This arises mainly from differences in the dipole moment function because the OH bonds have similar anharmonicities. The significant enhancement of fundamental intensities on hydrogen bonding is clear from both the $H_2O{\cdot}H_2O$ and $H_2O{\cdot}HNO_3$ results. This is also evident from a large increase of the first derivative of the dipole moment function along the OH_b bonds. It is meaningful to compare the intensity of $H_2O{\cdot}H_2O$ with 2 times the intensity of H_2O and the intensity of $H_2O{\cdot}HNO_3$ with the sum of the intensity of H_2O and HNO_3. The large increase in the fundamental intensity of $H_2O{\cdot}HNO_3$ and $H_2O{\cdot}H_2O$ compared to the individual molecules disappears completely in the $\Delta\nu_{OH} = 2$ region. The $H_2O{\cdot}HNO_3$ complex also shows increased OH-stretching intensity of the higher overtones $\Delta\nu_{OH} = 5$ and 6. However, one should note that these higher OH_b-stretching overtone transitions in $H_2O{\cdot}HNO_3$ are red-shifted to such an extent that they lie in the region of one lower quantum number of the H_2O unit in $H_2O{\cdot}HNO_3$. Simulated spectra of the OH-stretching transitions in the $\Delta\nu_{OH} = 4$ region for H_2O, $H_2O{\cdot}H_2O$, HNO_3, and $H_2O{\cdot}HNO_3$ are shown in Figure 4. The OH_b-stretching transition in the $\Delta\nu_{OH} = 5$ region of $H_2O{\cdot}HNO_3$ appears at around 13 900 cm^{-1}, slightly higher in energy than the $\Delta\nu_{OH} = 4$ OH_a- and OH_f-stretching transitions.

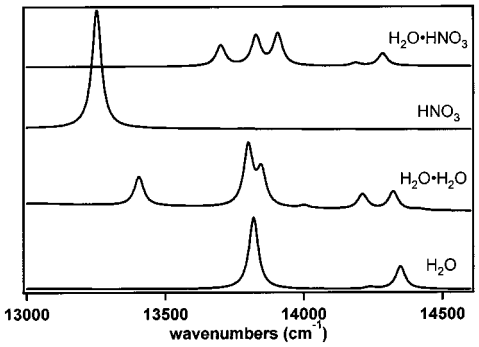

Figure 4. The simulated spectra of $H_2O{\cdot}HNO_3$, HNO_3, $H_2O{\cdot}H_2O$, and H_2O in the $\Delta\nu_{OH} = 4$ region. The $\Delta\nu_{OH} = 5$ OH_b-stretching transition in $H_2O{\cdot}HNO_3$ is seen in the top spectrum as the peak around 13 900 cm^{-1}. The spectra were calculated with the local-mode parameters from Tables 3 and 4 and QCISD/6-311++G(2d,2p) dipole moment functions. Each vibrational transition was convoluted with a Lorentzian with a fwhm of 40 cm^{-1}.

It is clear from Figures 3 and 4 that the OH-stretching spectrum of $H_2O{\cdot}HNO_3$ is significantly different than that of H_2O and HNO_3. Figure 4 clearly illustrates the red shifts of the OH_b- and OH_a-stretching overtone transitions in $H_2O{\cdot}HNO_3$ compared to the OH-stretching transitions in HNO_3 and H_2O, respectively. Vaida et al. have recently shown that the contribution to absorption of solar radiation from the water dimer depends largely on the line widths of the vibrational transitions and indicated that the largest contribution occurred in the fundamental and lower overtone regions.[17] The fundamental intensity of the $H_2O{\cdot}HNO_3$ complex is significantly enhanced. However, the atmospheric concentration of HNO_3 is low, and the abundance of the $H_2O{\cdot}HNO_3$ complex is even lower,[22] and it is unlikely that the $H_2O{\cdot}HNO_3$ complex will contribute significantly to the absorption solar radiation apart from perhaps in polluted areas with increased HNO_3 concentration.

The rate of OH radical production from the direct overtone photodissociation process depends on the intensity of the OH-stretching transitions (cross section) that have sufficient energy to dissociate the N−O bond. For HNO_3, the $\Delta\nu_{OH} = 6$ transition and higher rotational states of the $\Delta\nu_{OH} = 5$ transition have sufficient energy to generate OH radicals.[30,47] We have found that in the hydrated complex of nitric acid the intensity of the hydrogen-bonded OH_b-stretching intensity is enhanced; however, the transition is red-shifted such that a higher overtone is required to get the necessary energy for direct overtone photodissociation and thus will likely lead to a slower dissociation rate. Because there is little change in N−O bond length between HNO_3 and the $H_2O{\cdot}HNO_3$ complex, the N−O bond strength and energy required for dissociation is expected to be similar.

Conclusions

We have calculated the OH-stretching vibrational band frequencies and intensities of the monohydrated complex of nitric acid, $H_2O{\cdot}HNO_3$, and compared these with results obtained for H_2O, HNO_3, and $H_2O{\cdot}H_2O$. We have used the HCAO local-mode model with scaled ab initio-calculated local-mode parameters and ab initio-calculated dipole moment functions. The ab initio calculations were performed at the HF, B3LYP, and QCISD levels of theory with the 6-311++G(2d,2p) basis set. We investigated our computational approach for HNO_3 and compared our results with recently determined experimental intensities. For HNO_3, we find that these three methods provide

reasonable OH-stretching overtone intensities and that the use of even larger basis sets results in only modest changes in the intensities and little change in the calculated local-mode frequencies. We suggest that perhaps it is necessary to improve the potential beyond the Morse potential to obtain calculated OH-stretching intensities that agree better with the experimental values for HNO_3.

For the complexes, we show that the B3LYP theory overestimates the red shift of the hydrogen-bonded OH_b bond compared to experimental values for $H_2O{\cdot}H_2O$ and to the HF and QCISD results for both complexes. The HF and QCISD results are remarkably similar for the overtones, with the HF slightly underestimating and QCISD slightly overestimating the frequency red shift of the OH_b-stretching transition. However, electron correlation is required to get reasonable fundamental intensities. We suggest that our calculated OH-stretching spectra provide a guide as to which spectral regions are favorable for the detection of the spectra of the complexes.

We have investigated the effect that complexation of nitric acid with one water molecule has on the OH-stretching spectra and show that OH-stretching transitions change significantly both in peak positions and in intensity by complex formation. These calculated spectra of $H_2O{\cdot}HNO_3$ provide input parameters necessary in atmospheric models to estimate the absorption of solar radiation and production of OH radicals from the $H_2O{\cdot}HNO_3$ complex.

Because of the low atmospheric concentration of nitric acid, it is unlikely that $H_2O{\cdot}HNO_3$ will contribute significantly to solar absorption despite the wider peaks and the significantly increased fundamental OH-stretching intensity. The increase in OH-stretching intensity in $H_2O{\cdot}HNO_3$ is compensated by a large frequency red shift such that a higher overtone of the OH_b-stretching mode is required in the complex to provide sufficient energy for dissociation, and thus, significant enhancement of the OH radical production compared to HNO_3 is not likely.

Acknowledgment. I thank Professor Veronica Vaida, Daryl L. Howard, Timothy W. Robinson, Geoffrey R. Low, and Zimei Rong for helpful discussions. I am grateful to CIRES for a visiting faculty fellowship. The Marsden Fund administrated by the Royal Society of New Zealand and the University of Otago have provided funding for this research.

Supporting Information Available: A figure of the water dimer and of the nitric acid−water complex with the labeling used. Four tables with the fully optimized geometries of water, nitric acid, water dimer, and the nitric acid−water complex. Six tables with the ab initio-calculated local-mode parameters. Two tables with ab initio-calculated effective coupling coefficients for the various H_2O units. This material is available free of charge via the Internet at http://pubs.acs.org.

References and Notes

(1) Henry, B. R. *Acc. Chem. Res*. **1977**, *10*, 207.
(2) Henry, B. R. In *Vibrational Spectra and Structure*; Durig, J. R., Ed.; Elsevier: Amsterdam, 1981; Vol. 10, p 269.
(3) Mortensen, O. S.; Henry, B. R.; Mohammadi, M. A. *J. Chem. Phys*. **1981**, *75*, 4800.
(4) Child, M. S.; Lawton, R. T. *Faraday Discuss. Chem. Soc*. **1981**, *71*, 273.
(5) Sage, M. L.; Jortner, J. *Adv. Chem. Phys*. **1981**, *47*, 293.
(6) Mortensen, O. S.; Ahmed, M. K.; Henry, B. R.; Tarr, A. W. *J. Chem. Phys*. **1985**, *82*, 3903.
(7) Findsen, L. A.; Fang. H. L.; Swofford, R. L.; Birge, R. R. *J. Chem. Phys.* **1986**, *84*, 16.
(8) Tarr, A. W.; Swanton, D. J.; Henry, B. R. *J. Chem. Phys.* **1986**, *85*, 3463.
(9) Tarr, A. W.; Zerbetto, F. *Chem. Phys. Lett*. **1989**, *154*, 273.
(10) Kjaergaard, H. G.; Yu, H.; Schattka, B. J.; Henry, B. R.; Tarr, A. W. *J. Chem. Phys*. **1990**, *93*, 6239.
(11) Kjaergaard, H. G.; Turnbull, D. M.; Henry, B. R. *J. Chem. Phys*. **1993**, *99*, 9438.
(12) Kjaergaard, H. G.; Henry, B. R. *Mol. Phys*. **1994**, *83*, 1099.
(13) Kjaergaard, H. G.; Daub, C. D.; Henry, B. R. *Mol. Phys*. **1997**, *90*, 201.
(14) Kjaergaard, H. G.; Bezar, K. J.; Brooking, K. A. *Mol. Phys*. **1999**, *96*, 1125.
(15) Donaldson, D. J.; Orlando, J. J.; Amann, S.; Tyndall, G. S.; Proos, R. J.; Henry, B. R.; Vaida, V. *J. Phys. Chem. A* **1998**, *102*, 5171.
(16) Low, G. R.; Kjaergaard, H. G. *J. Chem. Phys*. **1999**, *110*, 9104.
(17) Vaida, V.; Daniel, J. S.; Kjaergaard, H. G.; Goss, L. M.; Tuck A. F. *Q. J. R. Meteorol. Soc.* **2001**, *127*, 1627.
(18) Ritzhaupt, G.; Devilin, J. P. *J. Phys. Chem.* **1977**, *81*, 521.
(19) Barnes, A. J.; Lasson, E.; Nielsen, C. J. *J Mol. Struct.* **1994**, *322*, 165.
(20) Canagaratna, M.; Phillips, J. A.; Ott, M. E.; Leopold, K. R. *J. Phys. Chem. A* **1998**, *102*, 1489.
(21) Koller, J.; Hadzi, D. *J. Mol. Struct.* **1991**, *247*, 225.
(22) Tao, F.-M.; Higgins, K.; Klemperer, W.; Nelson, D. D. *Geophys. Res. Lett.* **1996**, *23*, 1797.
(23) Ying, L.; Zhao, X. *J. Phys. Chem. A* **1997**, *101*, 6807.
(24) Toth, G. *J. Phys. Chem. A* **1997**, *101*, 8871.
(25) Staikova M.; Donaldson, D. J. *Phys. Chem. Chem. Phys*. **2001**, *3*, 1999.
(26) Zhang, H.; Roehl, C. M.; Sander S. P.; Wenneberg, P. O. *J. Geophys. Res.* **2000**, *105*, 14593.
(27) Brown, S. S.; Wilson, R. W.; Ravishankara, A. R. *J. Phys. Chem. A* **2000**, *104*, 4976.
(28) Vaida, V.; Headrick, J. E. *J. Phys. Chem. A* **2000**, *104*, 5401.
(29) Chylek, P.; Fu, Q.; Tso, H. C. W.; Geldart, D. J. W. *Tellus, Ser. A* **1999**, *51*, 304.
(30) Donaldson, D. J.; Frost, G. J.; Rosenlof, K. H.; Tuck, A. F.; Vaida, V. *Geophys. Res. Lett.* **1997**, *24*, 2651.
(31) Atkins, P. W. *Molecular Quantum Mechanics*, 2nd ed.; Oxford University: Oxford, U.K., 1983.
(32) Kjaergaard, H. G.; Henry, B. R. *J. Chem. Phys.* **1992**, *96*, 4841.
(33) Messiah, A. *Quantum Mechanics*; Wiley: New York, 1961; Vol. 1.
(34) Sowa, M. G.; Henry, B. R.; Mizugai, Y. *J. Phys. Chem.* **1991**, *95*, 7659.
(35) Press, W. H.; Flannery, B. F.; Teukolsky, S. A.; Vetterling, W. T. *Numerical Recipes in C*; Cambridge University: Cambridge, U.K., 1988.
(36) Frisch, M. J.; Trucks, G. W.; Schlegel, H. B.; Gill, P. M. W.; Johnson, B. G.; Robb, M. A.; Cheeseman, J. R.; Keith, T.; Petersson, G. A.; Montgomery, J. A.; Raghavachari, K.; Al-Laham, M. A.; Zakrzewski, V. G.; Ortiz, J. V.; Foresman, J. B.; Cioslowski, J.; Stefanov, B. B.; Nanayakkara, A.; Challacombe, M.; Peng, C. Y.; Ayala, P. Y.; Chen, W.; Wong, M. W.; Andres, J. L.; Replogle, E. S.; Gomperts, R.; Martin, R. L.; Fox, D. J.; Binkley, J. S.; Defrees, D. J.; Baker, J.; Stewart, J. P.; Head-Gordon, M.; Gonzalez, C.; Pople, J. A. *Gaussian 94*, revision D.4; Gaussian, Inc.: Pittsburgh, PA, 1995.
(37) Kjaergaard, H. G.; Robinson, T. W.; Brooking, K. A. *J. Phys. Chem. A* **2000**, *104*, 11297.
(38) Huisken, F.; Kaloudis, M.; Kulcke, A. *J. Chem. Phys.* **1996**, *104*, 17.
(39) Boys, S. F.; Bernardi, F. *Mol. Phys*. **1970**, *19*, 553.
(40) Curtiss, L. A.; Frurip, D. J.; Blander, M. *J. Chem. Phys.* **1979**, *71*, 2703.
(41) Niki, H.; Maker, P. D.; Savage C. M.; Breitenbach, L. P. *Chem. Phys. Lett.* **1977**, *45*, 564.
(42) Perrin, A.; Lado-Bordowsky, O.; Valentin, A. *Mol. Phys.* **1989**, *67*, 249.
(43) Huang, Z. S.; Miller, R. E. *J. Chem. Phys.* **1989**, *91*, 6613.
(44) Ziegler, T. In *Theoretical Treatments of Hydrogen Bonding*; Hadzi, D., Ed.; Wiley: Chichester, U.K., 1997; p 54.
(45) Guillory, W. A.; Bernstein, M. L. *J. Chem. Phys.* **1975**, *62*, 1058.
(46) Flemming, P. R.; Li, M.; Rizzo, T. R. *J. Chem. Phys.* **1991**, *94*, 2425.
(47) Sinha, A.; Van der Wal, R. L.; Crim, F. F. *J. Chem. Phys.* **1990**, *92*, 401.
(48) Sinha, A.; Van der Wal, R. L.; Crim, F. F. *J. Chem. Phys.* **1989**, *91*, 2929.
(49) Kjaergaard, H. G.; Henry, B. R.; Wei, H.; Lefebvre, S.; Carrington, T., Jr.; Mortensen, O. S.; Sage, M. L. *J. Chem. Phys.* **1994**, *100*, 6228.
(50) Wright, N. J.; Gerber, R. B.; Tozer, D. J. *Chem. Phys. Lett.* **2000**, *324*, 206.
(51) Schofield, D. P.; Low G. R. Unpublished work.
(52) Rong, Z.; Kjaergaard, H. G. Unpublished work.
(53) Perchard, J. P. *Chem. Phys.* **2001**, *266*, 109.
(54) Perchard, J. P. *Chem. Phys.* **2001**, *273*, 217.